2024 IEEE/RSJ International Conference on Intelligent Robots and Systems (IROS)
October 14-18, 2024. Abu Dhabi, UAE

Analysis of Lockable Passive Prismatic and Revolute Joints

Abdur Rosyid and Bashar El-Khasawneh

Abstract— **This paper analyzes the stresses, positional errors, and friction in lockable passive prismatic and revolute joints. The joints' locking mechanisms that use solenoids to trigger the locking action have a self-alignment capability. The stress analysis evaluates the strength and material deformation of the joints' components. The positional error analysis relates the clearances and contact deformations in the joints' assembly with the positional errors of the joints. The friction analysis investigates how the friction during the locking motion interacts with the joint load, the pushing force, and the locking acceleration. The stress analysis was performed analytically for simplified cases and by finite element analysis for cases involving complex geometries and nonlinear contact. The positional error and friction analyses were performed analytically by deriving the kinematic and dynamic equations. Discussions based on the analyses provide a deeper understanding of the behavior of lockable joints that applies not only to the specific joints discussed in this paper but also to other lockable joints working with similar principles.**

I. Introduction

Lockable joints can change their degrees of freedom (DOFs) by locking one or more of their DOFs. Such joints can be used in a reconfigurable robot to change the robot's joint topology. Such reconfiguration usually aims to change the robot's mobility, as in [1], or to change a certain performance measure of the robot, such as its workspace, as in [2]. While a lockable active joint can be as simple as fixing one or more of its DOFs by locking the joint actuators, a lockable passive joint may require a complex design. The design of lockable passive joints varies depending on the locking mechanisms used.

In [3], we proposed novel lockable passive joints that use male and female components as the locking mechanisms. These components are pin-and-hole mechanism for lockable passive prismatic (P) joint and dog clutch mechanism for lockable passive revolute (R), universal (U), and spherical (S) joints. Such locking mechanisms are suitable for discrete locking that is required in some applications. Conical features are added to those locking mechanisms to provide self-alignment capability. The dog clutch mechanism for the lockable passive R, U, and S joints is identical, leading to a modular design of the lockable joints.

Among the challenges in designing and manufacturing a lockable joint is the locking accuracy. In a lockable joint that uses a male-and-female locking mechanism such as a locking pin and a dog clutch, the locking accuracy is affected by rigid-body clearance and material deformation. The rigid-body clearance, defined as the clearance in the absence of material deformation, is frequently inevitable since the mating parts need to have a sliding motion between each other. On the other hand, additional clearance may occur due to material deformation caused by loading exerted on the locking parts. All these clearances are typically not considered in the topological design and rigid body kinematic model of a lockable joint. Nevertheless, the presence of such clearances in an actual lockable joint reduces the accuracy of the joint.

While some studies have investigated the effect of clearance, material deformation, and friction in standard joints [4 - 8], we need help finding enough studies that evaluate the effect of clearance, material deformation, and friction in lockable joints. While the standard joints have relatively simple geometry, the lockable joints we proposed have relatively complex geometry due to the locking mechanisms with self-alignment features in the joints. For this reason, this paper presents a study focusing on the clearance, material deformation, and friction in the locking mechanisms of the proposed lockable joints, to complement the previous analyses on the standard joints. This is the novelty as well as the scope limit of this paper. The positional errors in the lockable joints caused by the clearance and the material deformation will be discussed. The stresses will also be analyzed as the material deformation is caused by stresses working in the joint components. The stresses working in mating components will take the contact into account. The friction analysis will focus on the sliding friction that occurs when solenoids push the female locking components into the male locking components.

Although we proposed four lockable passive joints, there are only two different locking mechanisms used in all the proposed joints. This is because the proposed lockable passive R, U, and S joints have an identical locking mechanism since the U and S joints are composed from two and three R joints, respectively. This locking mechanism is only different from the locking mechanism used in the lockable passive P joint. The analysis will be performed analytically and numerically, depending on the applicability of each approach. Based on the analysis, the behavior of the proposed lockable joints will be discussed. Although the analysis is performed to specific lockable joints, similar analysis can be performed to other types of lockable joints that use similar working principles.

The remainder of the paper will be organized as follows. Sections II and III will analyze the locking mechanisms in the lockable passive P and R joints, respectively. Each section will analyze the stresses and deformations, the clearance and positional error, and the friction between locking components of the lockable passive P and R joints. Section IV presents some discussions based on the performed analysis. Finally, Section V concludes the paper.

Abdur Rosyid is with Center for Autonomous Robotic Systems (KUCARS), Mechanical and Nuclear Engineering Department, Khalifa University of Science & Technology, P.O. Box 127788, Abu Dhabi, UAE (e-mail: abdur.patrum@ku.ac.ae)

Bashar El-Khasawneh is with Center for Autonomous Robotic Systems (KUCARS), Mechanical and Nuclear Engineering Department, Khalifa University of Science & Technology, P.O. Box 127788, Abu Dhabi, UAE (phone: +97123124157, e-mail: bashar.khasawneh@ku.ac.ae)

II. Analysis of Lockable Passive Prismatic Joint

The main components of the locking mechanism are the locking pin and hole, with a tapering end in each to provide self-alignment capability. Fig. 1 shows the CAD model of the lockable passive P joint in an exploded view along with its 3D-printed prototype. The figure shows that a standard rail-slider mechanism that serves as a standard P joint is turned to a lockable passive P joint by adding the shown locking mechanism. The solenoid used in the prototype has a stroke distance of 35 mm. It requires a 12V power supply with a maximum of 8A current draw.

Fig. 1. (a) The CAD model in exploded view and (b) the 3D-printed prototype of the passive prismatic lockable joint

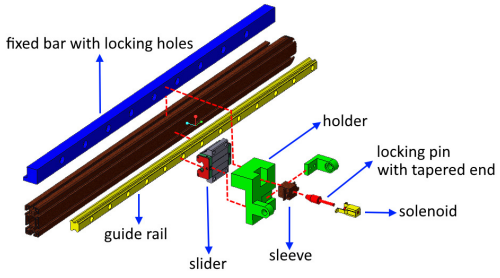

(a)

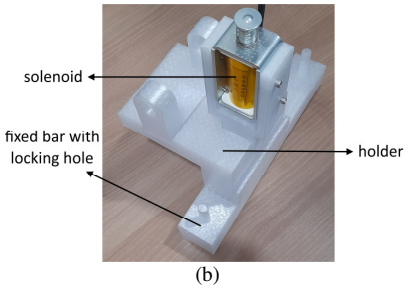

(b)

In the reconfigurable parallel robot we proposed in [2], as an example, the slider that moves along its rail is subjected to a load exerted by the limb it carries. This load is resolved into two components: one component in the direction of the slider's motion along the rail, namely F_m, and another component perpendicular to the rail. The former load is constrained by the locking mechanism, whereas the latter load is transferred to the rail structure.

A. *Stress analysis*

The cross-section view of the locking pin and hole is depicted in Fig. 2. A perfect pin with a diameter d_2 equal to the hole's diameter is shown in Fig. 2(a). An imperfect pin with a diameter d_2^* less than the hole's diameter d_2 is shown in Fig. 2(b). The difference between d_2 and d_2^* results in a radial clearance δ_c between the pin and the hole. The figure also shows the force F_m exerted on the locking pin. Since the force F_m works transversally on the pin, it results in a shearing action to the pin. This shearing action can be modeled by fixing the locking hole and applying the shearing force F_m to the pin. With a perfect pin, the model can be simplified by considering the shear in the cylindrical part of the pin. According to the mechanics, the average shear stress τ_{avg} that has a uniform magnitude across the pin cross-section area A is given by:

Fig. 2. The cross section views of the lockable passive P joint (a) without a radial clearance and (b) with a radial clearance

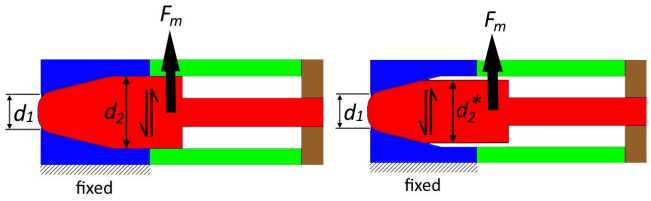

(a) (b)

$$\tau_{avg} = \frac{F_m}{A} = \frac{F_m}{\frac{\pi}{4}{d_2}^2} \quad (1)$$

In reality, the shear force profile is not uniform across A. For a solid circular cross section, the maximum of this shear stress profile is given by:

$$\tau_{max} = \frac{4F_m}{3A} = \frac{4F_m}{\frac{3\pi}{4}{d_2}^2} \quad (2)$$

With an imperfect pin as shown in Fig. 2(b), Eqs. (1) and (2) should be modified by substituting d_2 with d_2^*.

With the prototype having d_2 = 20 mm, using (1) and (2), the average and maximum shear stresses caused by a shear force F_m = 100 N exerted on a perfect pin are $\tau_{avg} = 3.1831 \times 10^5$ Pa and $\tau_{max} = 4.2441 \times 10^5$ Pa.

Since the force F_m presses the pin to the hole surface, there is a contact between the pin and the hole surface. This causes a contact stress that can be added to the shear stress evaluated in (2) to obtain the maximum shear stress that considers contact. Using finite element analysis (FEA) in ANSYS, the maximum shear stress considering the contact between the perfect pin and the hole is shown in Fig. 3(a). The contact is modeled as a frictionless contact. As shown, the computed maximum shear force is $\tau_{max} = 4.2877 \times 10^5$ Pa. This result is 1.0161 percent larger than the analytical result calculated using (2) that does not take contact into account. With an

Fig. 3. The maximum shear stress in (a) the perfect lockable passive P joint and (b) the imperfect lockable passive P joint, with contact between the pin and the hole taken into account

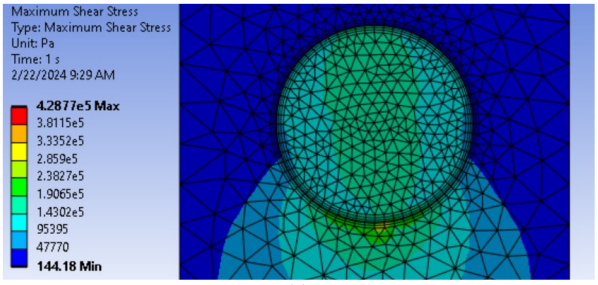

(a)

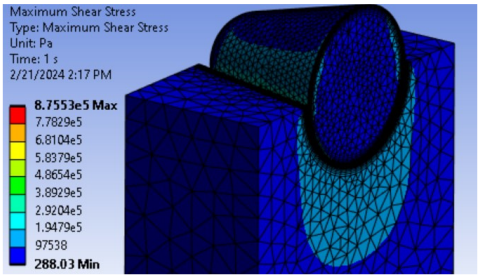

(b)

imperfect pin, the contact only occurs in the conical part of the pin. Accordingly, the maximum shear stress in the imperfect pin can be evaluated by using only the conical part and its corresponding hole, as shown in Fig. 3(b). With a frictionless contact between the conical part of the pin and the conical hole, the maximum shear stress computed in ANSYS is $\tau_{max} = 8.7553 \times 10^5$ Pa. This is roughly two times larger than the value obtained for a perfect pin.

B. *Positional error analysis*

As discussed earlier, the difference between d_2 and d_2^* results in a radial clearance δ_c between the pin and the hole. Fig. 4(a) shows the locking mechanism when the solenoid pushes the pin toward the hole with a sufficient force F_{pi}, even with the presence of force F_m, such that the pin keeps itself aligned with the center axis. In this condition, we can assume $\delta_{c1} = \delta_{c2}$. The force F_{po} shown in the figure is the reaction force given by the conical hole to balance the force F_{pi} in a static condition. When F_m is so large that F_{pi} cannot maintain the pin alignment with the center axis, the pin is radially offset as shown in Figs. 4(b) and 4(c). If the offset pin is not in contact with the hole surface, as depicted in Fig. 4(b), the radial offset is given by:

$$\delta_c = \delta_{c1} - \delta_{c2} \tag{3}$$

If the offset pin is in contact with the hole surface, as depicted in Fig 4(c), the radial offset without considering the material deformation due to contact is given by:

$$\delta_c = \delta_{c1} + \delta_{c2} \tag{4}$$

A certain positive value of δ_c is required to enable the sliding motion of the pin along the hole. This positive value should result in a sliding fit between the pin and the hole.

Fig. 4. The radial clearance (a) when the pin keeps its position in the center, (b) when the pin is radially offset but is not in contact with the the hole surface, and (c) when the pin is radially offset and in contact with the the hole surface

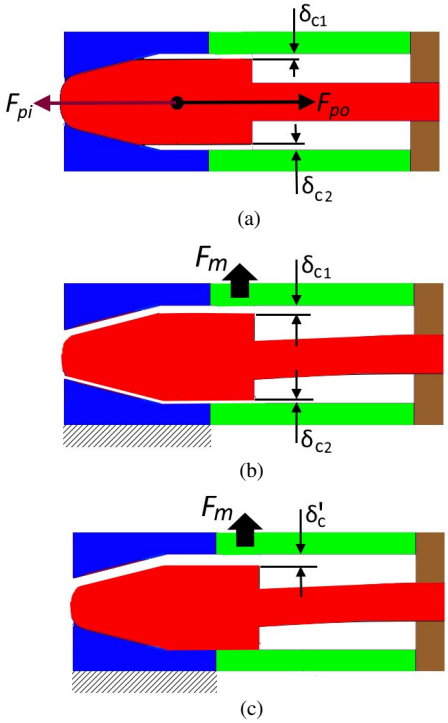

In general, the material deformation namely δ_m can be written in the radial direction as:

$$\delta_m = \delta_{ms} + \delta_{mb} + \delta_{mc} \tag{5}$$

where the terms in the right-hand side of (5) indicate the material deformations due to shear, bending, and contact, respectively. If the offset pin is not in contact with the hole surface, $\delta_{mc} = 0$ and hence (3) can be rewritten as:

$$\delta_c = \delta_{c1} - \delta_{c2} = \delta_{ms} + \delta_{mb} \tag{6}$$

In contrast, a non-zero δ_{mc} should be considered if the offset pin is in contact with the hole surface. In this case, the radial offset δ_c' that considers the contact deformation is obtained by adding the contact deformation to the radial offset neglecting the contact deformation given by (4), i.e.:

$$\delta_c' = \delta_c + \delta_{mc} = \delta_{ms} + \delta_{mb} + \delta_{mc} \tag{7}$$

The discussed radial offset defines the positional error of the lockable passive P joint. It can be reduced by minimizing the difference between the diameters of the pin and the hole, using a stronger material, enlarging the diameter of the pin shank, minimizing the force F_m exerted on the locking mechanism, and enlarging the pushing force F_{pi} provided by the solenoid.

C. *Friction analysis*

The pin and hole friction can be analyzed in two stages. The first stage occurs when the pin is not concentric with the hole during the initial motion of the pin, as shown in Fig. 5. In this stage, the conical part of the pin slides along the opening edge of the hole while the pin moves diagonally toward the center axis of the hole. For easier self-alignment, the opening edge of the hole can be filleted, as shown in the figure. This also reduces the friction due to the absence of sharpness in the opening edge of the hole. The pushing force F_{pi} from the solenoid and the force F_m exerted by the limb compose the resultant force F, i.e., $F = F_{pi} + F_m$. This force is exerted on the contact point between the pin and the hole opening edge. This force can be resolved into the normal component F_n and the tangential component F_t. Please note that the normal and tangential directions here may change with the motion of the pin. Let θ be the angle between F and the normal. The normal and tangential directions depend on the angle θ. The normal component F_n is given by:

$$F_n = F \cos\theta \tag{8}$$

The static and Coulomb friction forces depend on the normal force N and the friction coefficients of the materials in contact. The normal force N is a reaction to the force component F_n,

Fig. 5. Free body diagrams of the pin motion in the first stage in (a) the first scenario and (b) the second scenario

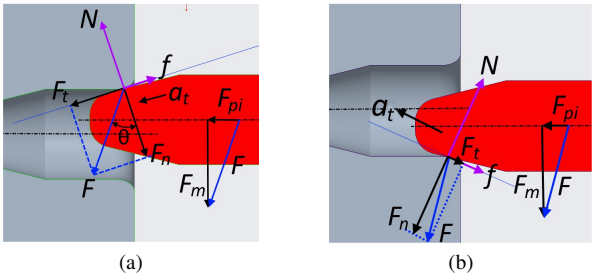

i.e., $N = -F_n$. While the pin moves in the tangential direction, the following equation of motion applies:

$$F_t - f = F \sin\theta - f = m\, a_t \tag{9}$$

where f is the friction force, whereas m and a_t are the mass and the acceleration (in the tangential direction) of the pin, respectively. From (9), it is obvious that the pin only moves when a_t is not zero. When the pin stops in this stage, i.e., $a_t = 0$, Eq. (9) is reduced to:

$$F_t = F \sin\theta = f \tag{10}$$

Fig. 5 shows two scenarios in which the pin starts entering the hole from different offset positions. In the first scenario, shown in Fig. 5(a), the pin can enter the hole and align itself more easily as the direction toward the center axis is the same as the direction of the force F_m exerted by the limb. In the second scenario, shown in Fig. 5(b), it is harder to insert and align the pin with the hole as the force F_m resists that action. Therefore, if there should be an offset prior to the insertion of the pin into the hole, it is better to have the first scenario.

The second stage of friction analysis occurs when the pin is aligned with the hole and slides along the hole, as shown in Fig. 6 until it stops. The normal force N in this stage is a reaction to the sum of the force F_m exerted by the limb and a contact force F_c that depends on the contact intensity between the pin and the hole. This can be written as:

$$N = -(F_m + F_c) \tag{11}$$

Fig. 6. Free body diagram of the pin motion in the second stage

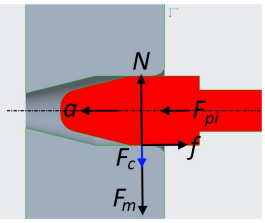

Recalling that the clearance δ_c cannot be zero to enable a sliding motion of the pin along the hole, the smaller the value of δ_c, the larger the value of F_c and accordingly the larger the normal force N. Since N becomes larger, the friction also becomes larger.

In this stage, the effective pushing force $F_{pi}{}'$ is defined as the pushing force F_{pi} subtracted by the friction force f. In the direction of pin's motion, the following equation of motion applies:

$$F'_{pi} = F_{pi} - f = m\, a \tag{12}$$

where m and a are the mass and the acceleration of the pin. Since the friction works in the opposite direction to the pushing force F_{pi} given by the solenoid, a larger friction reduces the effective pushing force. A larger friction force without an increase in the pushing force F_{pi} will also reduce the acceleration of the pin, leading to a reduced speed of the pin motion. Eq. (12) also implies that the pin only moves when a is not zero. When the pin stops in this stage, then $F_{pi} = f$.

III. Analysis of Lockable Passive Revolute Joint

Fig. 7 shows the CAD model of the lockable passive R joint in an exploded view along with its 3D-printed prototype.

Fig. 7. (a) The CAD model in exploded view and (b) the 3D-printed prototype of the lockable passive R joint

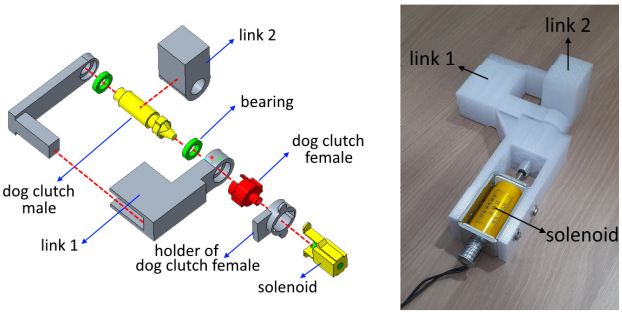

(a) (b)

Fig. 8. 3D-printed prototypes of (a) the lockable passive U joint and (b) the lockable passive S joint

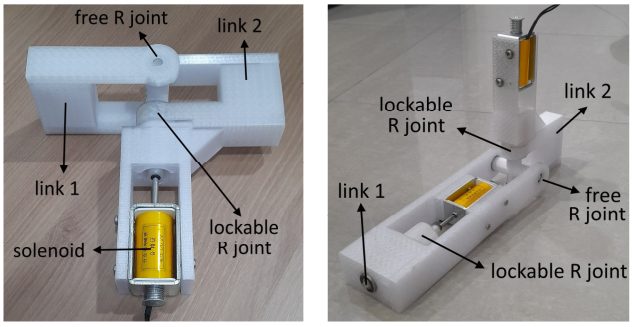

(a) (b)

The dog clutch mechanism serves as the locking mechanism. The male and female parts of the dog clutch have cylindrical and conical tapering features to provide self-alignment capability. Fig. 8 shows the 3D-printed prototypes of the lockable passive U and S joints that use identical locking mechanisms in a modular fashion. The solenoids used in the prototypes of the lockable passive R, U, and S joints are identical to that used in the prototype of the lockable passive P joint. Since the locking mechanisms in the U and S joints are identical to that in the R joint, the analysis will be performed only on the R joint.

A. Stress analysis

To evaluate the strength of each component of the locking mechanism, stress and deformation analysis in ANSYS is performed to individual components, namely dog clutch male part, dog clutch female part, and slider. As shown in Fig. 9 that depicts the cross-section view of the locking mechanism, the slider is a part of the dog clutch female. It slides along its groove when the solenoid pushes or pulls the dog clutch female. When the dog clutch is in locked state, the load from

Fig. 9. Cross-section view of the locking mechanism in the lockable passive R joint

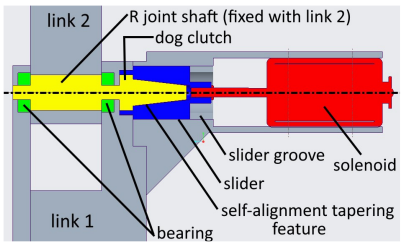

link 2 is sequentially transferred to the dog clutch male, the dog clutch female, the slider, the slider groove (the holder of dog clutch female), and link 1 structure. The deformation is analyzed by using steel that has Young modulus of 2×10^{11} Pa as the material of all the components.

When the joint is locked, the dog clutch male can be modeled by fixing the surfaces of its jaws that have contact with the dog clutch female jaws while applying a moment about its center line, as shown in Fig. 10(a). Assuming a moment of 150 Nm applied to the joint, the equivalent stress and deformation in the dog clutch male are shown in Fig. 10(a). The engaged dog clutch female can be modeled by fixing the slider while applying coupling forces to its jaws. With the moment of 150 Nm working in the joint and the radius of the jaws of 0.015 m, the coupling forces F_r of 10,000 N are obtained by dividing the moment by the radius of the jaws. The equivalent stress and deformation in the dog clutch female are shown in Fig. 10(b). Finally, the equivalent stress and deformation in the slider and its surroundings, including the tapering hole, shown in Fig. 10(c), can be evaluated by fixing the surfaces of the slider that have contact with the slider groove during the application of the moment loading.

Fig. 10. The equivalent stresses and deformations in (a) the dog clutch male, (b) the dog clutch female, and (c) the slider and its surrounding

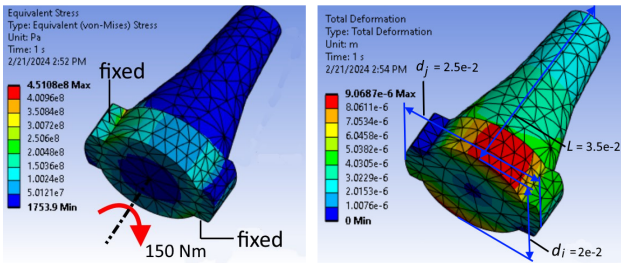

(a)

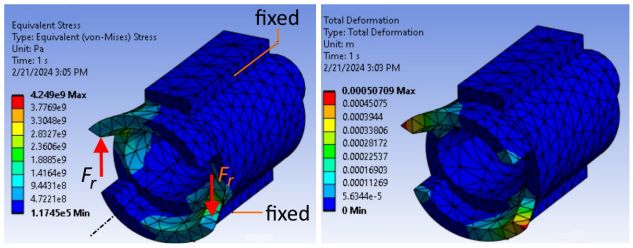

(b)

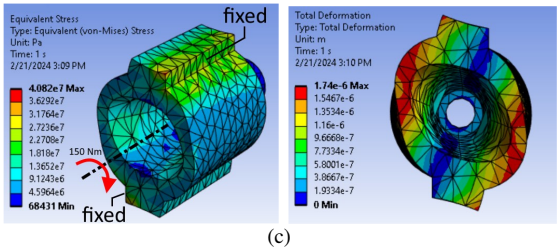

(c)

After the stress and deformation analysis is performed to the individual components, the stress and deformation analysis is performed to the mating components, with contact taken into consideration. Using the same material and assuming a frictionless contact, the equivalent stress and deformation in the dog clutch are shown in Fig. 11(a). The analysis is performed by fixing the dog clutch female while applying a moment of 150 Nm to the dog clutch male. The equivalent

Fig. 11. The equivalent stresses and deformations in (a) the assembly of the dog clutch male and female and (b) the assembly of the elliptical conical part mating with its elliptical conical hole and the slider mating with its groove, with contact between the parts taken into account

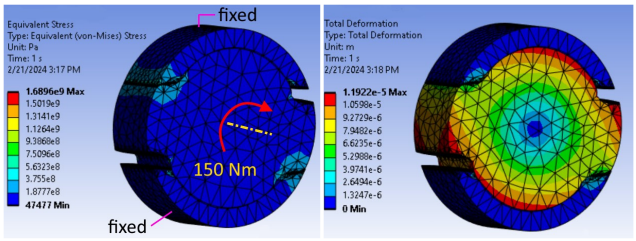

(a)

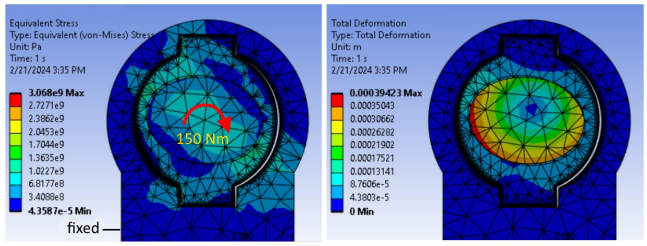

(b)

stress and deformation in the assembly of the elliptical conical part mating with its elliptical conical hole and the slider mating with its groove/housing are shown in Fig. 11(b). This analysis involves three components in an assembly. The housing is fixed, the dog clutch female is free to rotate, and the elliptical conical part is subject to a moment load of 150 Nm.

B. Positional error analysis

Since the locking mechanism assembly consists of the dog clutch male, the dog clutch female along with the slider, and the housing with the slider groove, the clearances between these parts in the assembly should be considered in the positional error analysis. Fig. 12(a) depicts the clearance between the dog clutch male and female. The clearance can be written as:

$$\delta_j = \delta_{j1} + \delta_{j2} = w_j^* - w_j \tag{13}$$

The clearance δ_j should be larger than zero to enable a sliding motion of the dog clutch female to its male. However, a too large value of δ_j causes a large error of the joint in its locked state. This is because the clearance δ_j results in an angular offset α_j in the dog clutch mechanism as shown in Fig. 12(b). The larger the clearance δ_j, the larger the angular offset α_j. Referring to Fig. 12(b), we can write:

$$\frac{\alpha_j}{2\pi} = \frac{\delta_j}{\pi d_j} \tag{14}$$

From (14), the angular offset α_j can be written as:

Fig. 12. (a) The clearance between the dog clutch male and female and (b) the resulting angular offset due to the clearance

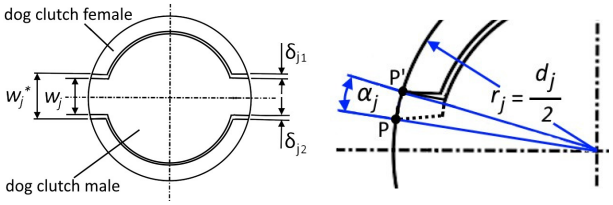

(a) (b)

$$\alpha_j = \frac{2\,\delta_j}{d_j} \tag{15}$$

Fig. 13(a) depicts the clearance between the slider and its groove in the housing (the holder of the dog clutch female). The clearance can be written as:

$$\delta_s = \delta_{s1} + \delta_{s2} = w_s^* - w_s \tag{16}$$

Referring to Fig. 13(b), we can write:

$$\frac{\alpha_s}{2\pi} = \frac{\delta_s}{\pi d_j} \tag{17}$$

From (17), the angular offset α_s can be written as:

$$\alpha_s = \frac{2\,\delta_j}{d_s} \tag{18}$$

Fig. 13. (a) The clearance between the slider and its groove and (b) the resulting angular offset due to the clearance

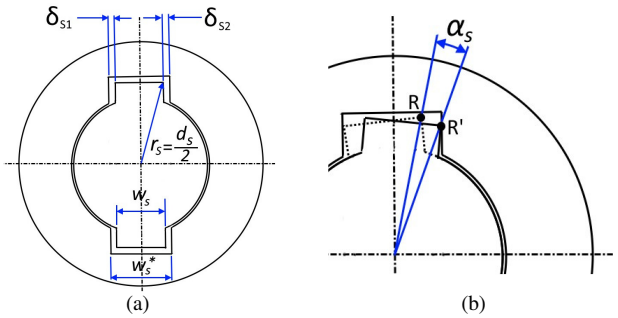

The total angular offset in the locking mechanism of the lockable passive R joint is given by:

$$\alpha_R = \alpha_j + \alpha_s \tag{19}$$

To this point, the discussed angular offsets do not take into account the material deformations due to contact between the parts. If the material deformations due to the contact are taken into account, the clearances should be modified to the following:

$$\delta_j{}' = \delta_j + \delta_{mcj} \tag{20}$$

$$\delta_s{}' = \delta_s + \delta_{mcs} \tag{21}$$

where the apostrophe mark indicates the clearance that takes into account the material deformation due to contact. The terms δ_{mcj} and δ_{mcs} are the material deformations due to contact in the dog clutch assembly and the slider–groove assembly, respectively. Accordingly, the angular offsets should also be modified to the following approximations:

$$\alpha_j{}' = \frac{2\,\delta_j{}'}{d_j} \tag{22}$$

$$\alpha_s{}' = \frac{2\,\delta_j{}'}{d_s} \tag{23}$$

Finally, the total angular offset that takes into account the material deformation due to contact can be written as:

$$\alpha_R{}' = \alpha_j{}' + \alpha_s{}' \tag{24}$$

C. *Friction analysis*

The self-alignment in the lockable passive R joint is guided by two conical features, namely the cylindrical and elliptical conical features. The cylindrical conical feature brings the dog clutch male from an offset initial position to be concentric with the dog clutch female. Subsequently, the elliptical conical feature guides the dog clutch male jaws to the dog clutch female jaws. Referring to Fig. 14, assume the dog clutch male is already concentric with the dog clutch female, but their jaws are still not aligned. Suppose the orientation of the jaws is initially offset by θ_a. At the initial position, the dog clutch male and female make contact at point S. As the solenoid pushes the dog clutch female, the contact point moves from point S to point E along the indicated arrow line. When this self-alignment motion reaches point E, the conical features of the dog clutch male and females are aligned, and accordingly, the dog clutch jaws are aligned and engaged. Please note that the initial angle θ_a should be less than $\pi/2$. The less the value of θ_a, the easier and faster the self-alignment is.

Fig. 14. Projection views of the dog clutch male and female when their elliptical conical features self-align their orientation

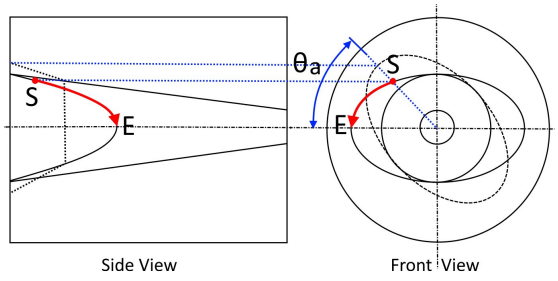

During the sliding contact between the conical features of the dog clutch male and female from point S to point E, a sliding friction occurs. The sliding friction force f is mainly affected by the normal force N and the friction coefficient of the materials. Fig. 15 shows the free body diagram of the dog clutch at a point namely P along the sliding line $\overline{SE}$. The free body diagram is presented in two projective views for convenience since the vectors are working in three-dimensional space. From the free body diagram, the following equations of motion apply:

$$N = F_n + m\,a_n = F\cos\theta + m\,a_n \tag{25}$$

$$F_t - f = F\sin\theta - f = m\,a_t \tag{26}$$

where m is the mass of the dog clutch female pushed by the solenoid whereas a_n and a_t are the normal and tangential components of the dog clutch female acceleration a, respectively. Eq. (25) shows that the normal force N is not only dictated by the F_n, but also by the normal component of the acceleration, a_n.

Fig. 15. Free body diagram during a sliding contact between the elliptical conical features

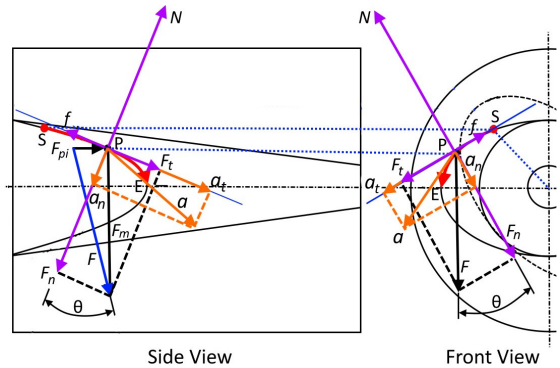

IV. Discussions

The stress analysis in Section II.A confirms that considering contact between mating components increases the computed stress. This is because the contact stress is added to the stress in the individual loaded component. Accordingly, the material deformation increases when contact between mating components is taken into account because contact stress, in general, results in contact deformation. It is well known in mechanics that the contact stress and deformation are affected by the loading, the material properties, and the contact geometry.

The stress analysis of the P joint locking mechanism also shows that a perfect pin-and-hole assembly leads to significantly less stress compared with an imperfect assembly caused by the clearance between the pin and the hole. This is because the load is only handled by the tapered part of the pin in the latter case. Therefore, it is important to minimize the clearance between the pin and the hole such that both the cylindrical and tapered parts of the pin handle the joint load.

The locking components in the P joint are mainly subject to shear and bending, whereas the locking components in the R joint are mainly subject to twist. The stress analysis of both the joints shows that the type of joint loading affects the stress and deformation profiles in their locking components. In particular, attention should be paid to thin features in the locking components, such as the locking jaws and the thinner elliptical conical wall in the R joint.

As a stress analysis method, we introduced two main steps in analyzing all the joints. The first is stress analysis of the individual components to evaluate the strength (in terms of stress and deformation) in the worst-case scenario. The second is stress analysis of the mating components, i.e., the assembly, by considering the contact between components. This can also indicate the weakest component in the assembly and the expected deformation within the assembly.

The kinematics of the positional error derived in this paper clearly shows that the clearance between the mating components is directly propagated to the joint positional error. Therefore, a clearance larger than required leads to an unexpected joint positional error. Furthermore, the positional error analysis, as well as the stress/deformation analysis, shows that the number of components in the locking mechanism, in general, increases the positional error of the joint. This is because the joint positional error is the sum of the error introduced by the clearances between the mating components. In fact, mating components intended to make sliding motion cannot have a zero clearance.

It is also important to consider the material deformation due to contact into the resulting joint positional error, in addition to the positional error due to rigid-body clearance, i.e., clearance without material deformation. It was shown in this paper that the material deformation considering the contact can be conveniently evaluated using FEA. In general, the positional error can be reduced by minimizing the rigid-body clearance, using a stronger material, optimizing the locking component geometry, minimizing the joint load, and enlarging the pushing force provided by the solenoid. The amplification of the joint positional error from the joint space to the task space of a mechanism/robot can be evaluated through some input-output sensitivity indices such as the Jacobian condition number. This is beyond the scope of this paper.

The dynamic models involving the friction in the locking mechanism show that the friction is affected by the joint load, the pushing force provided by the solenoid, the inertia of the locking component, the acceleration of the locking component during its locking motion, the geometry of the locking components, the initial position before self-alignment, and the friction coefficient of the mating materials.

V. Conclusion

The 3D-printed prototypes of the proposed lockable passive P, R, U, and S joints were presented in this paper. Afterward, the stress/deformation, positional error, and friction analyses were performed on the locking mechanisms of the joints. The behavior of the joints was discussed based on the analyses. In the future, the proposed joints will be re-prototyped by using steel as their material to optimize the strength and accuracy of the joints, and subsequently, similar analyses can be validated by experiments and more quantitative conclusions can be drawn from the experiments.

Acknowledgment

The authors would like to acknowledge Khaleefa Al Mehairbi, Shaik Khizer, and Pityas Welday for their help in refining the CAD models of the lockable passive joints and prototyping the joints.

References

[1] Y. Zhao, Y. Jin, H. Anderson, and C. Higgins, A new reconfigurable parallel mechanism using novel lockable joints for large scale manufacturing, Robotics and Computer-Integrated Manufacturing, vol. 82, 102542, 2023, https://doi.org/10.1016/j.rcim.2023.102542

[2] A. Rosyid, C. Stefanini, and B. El-Khasawneh, A Novel Reconfigurable 3-DOF Parallel Kinematics Machine, ASME Journal of Mechanisms and Robotics, vol. 16, no. 2, 021005, 2024, https://doi.org/10.1115/1.4056683

[3] A. Rosyid and B. El-Khasawneh, Novel Lockable Passive Joints for Joint Locking-based Reconfigurable Mechanisms, International Mechanical Engineering Congress and Exposition (IMECE2023), October 29-November 2, 2022, New Orleans, Louisiana, https://doi.org/10.1115/IMECE2023-112738

[4] Z. F. Bai and Y. Sun, A study on dynamics of planar multibody mechanical systems with multiple revolute clearance joints, European Journal of Mechanics - A/Solids, vol. 60, pp. 95-111, 2016, https://doi.org/10.1016/j.euromechsol.2016.06.009

[5] J. Li, H. Huang, S. Yan, and Y. Yang, Kinematic accuracy and dynamic performance of a simple planar space deployable mechanism with joint clearance considering parameter uncertainty, Acta Astronautica, vol. 136, pp. 34-45, 2017, https://doi.org/10.1016/j.actaastro.2017.02.027

[6] H. Tan, L. Li, Q. Huang, Z. Jiang, Q. Li, Y. Zhang, and D. Yu, Influence of two kinds of clearance joints on the dynamics of planar mechanical system based on a modified contact force model, Scientific Reports, vol. 13, 20569, 2023, https://doi.org/10.1038/s41598-023-47315-1

[7] Q. Tian, P. Flores, and H. M. Lankarani, A comprehensive survey of the analytical, numerical and experimental methodologies for dynamics of multibody mechanical systems with clearance or imperfect joints, Mechanism and Machine Theory, vol. 122, pp. 1-57, 2018, https://doi.org/10.1016/j.mechmachtheory.2017.12.002

[8] A. Rosyid and B. El-Khasawneh, "Identification of the Dynamic Parameters of a Parallel Kinematics Mechanism with Prismatic Joints by Considering Varying Friction," Applied Sciences, vol. 10, no. 14, 4820, https://doi.org/10.3390/app10144820